Domain Stability and Metal-Induced Folding of Calcium- and Integrin-Binding Protein 1†

Aaron P. Yamniuk,‡ Dylan M. Silver,‡ Kathryn L. Anderson,‡ Stephen R. Martin,§ and Hans J. Vogel*,‡

Structural Biology Research Group, Department of Biological Sciences, University of Calgary, 2500 University Drive N.W., Calgary, AB, Canada, T2N 1N4, and Division of Physical Biochemistry, National Institute for Medical Research, Mill Hill, London, NW7 1AA, U.K.

Received January 30, 2007; Revised Manuscript Received April 11, 2007

ABSTRACT: It is widely accepted that a pair of EF-hands is the functional unit of typical four EF-hand proteins such as calmodulin or troponin C. In this work we investigate the structure and stability of the four EF-hand domains in the related protein calcium- and integrin-binding protein 1 (CIB1) in the presence and absence of Mg^{2+} or Ca^{2+}, to determine if similar EF-hand interactions occur. The backbone structure and flexibility of CIB1 were first studied by NMR spectroscopy, and these studies were complimented with steady-state fluorescence spectroscopy and chemical denaturation experiments using mutant CIB1 proteins having single Trp reporter groups in each of the four EF-hand domains EF-I (F34W), EF-II (F91W), EF-III (L128W), and EF-IV (F173W). We find that Mg^{2+}-CIB1 adopts a well-folded structure similar to Ca^{2+}-CIB1, except for some conformational heterogeneity in the C-terminal EF-IV domain. The structure of apo-CIB1 is significantly more dynamic, especially within EF-II, EF-III, and a partially unfolded EF-IV region, but the N-terminal EF-I region of apo-CIB1 has a well-ordered and more stable structure. The data reveal significant communication between the N- and C-lobes of CIB1, and show that transient intermediate conformations are formed along the unfolding pathway for each form of the protein. Collectively the data demonstrate that the communication between the paired EF-hand domains as well as between the N- and C-lobes of CIB1 is distinct from the ancestral proteins calmodulin and troponin C, which might be important for the unique function of CIB1 in numerous biological processes.

Calcium- and integrin-binding protein 1 (CIB1,[1] calmyrin, KIP1) is a ubiquitous EF-hand Ca^{2+}- and Mg^{2+}-binding protein with several putative functions in humans, including proposed roles in hemostasis, apoptosis, and the DNA damage response; for a recent review see ref *1*. Like many other members of the calmodulin (CaM) superfamily, CIB1 consists of 4 "helix−loop−helix" EF-hand domains that can be divided into an N-lobe (EF-I/EF-II) and a C-lobe (EF-III/EF-IV). In addition, CIB1 has a myristoylated N-terminal extension that can target CIB1 to the cytoplasmic membrane (*2*), and a C-terminal extension which folds back on the protein and increases target protein binding specificity (*3*). Due to several key mutations and small insertions in the metal-binding loops of EF-I and EF-II, the N-lobe EF-hands are incapable of binding divalent metal ions. EF-I in particular could be considered an "EF-hand-like" domain, since an 8 residue insertion in the metal-binding loop results in a noncanonical fold for this domain. In contrast, both C-lobe sites conform to the canonical EF-hand sequence, with EF-IV being a high affinity Ca^{2+}-specific site and EF-III being a lower affinity Ca^{2+}- and Mg^{2+}-binding site (*4*). The noncooperative Mg^{2+}- and Ca^{2+}-binding behavior suggests that the communication between EF-III and EF-IV of CIB1 may be distinct from the cooperative metal-binding and conformational changes that generally occur in paired EF-hand domains (*5*, *6*).

We have previously shown that metal-free CIB1 (apo-CIB1) has some secondary structure, but unstable tertiary structure (*4*). Ca^{2+} binding to apo-CIB1 stabilizes the entire structure of the protein, with the N- and C-lobes of Ca^{2+}-CIB1 forming distinct globular units that interact with each other predominantly between EF-II and EF-III (*3*, *7*). Mg^{2+} binding also stabilizes a large portion of the protein structure, but an as yet unidentified region of Mg^{2+}-CIB1 appears to retain some of the flexible properties of apo-CIB1 (*4*). Since the intracellular Mg^{2+} and Ca^{2+} concentrations would dictate the metal-bound state of CIB1 *in vivo*, it is clear that Mg^{2+}-CIB1 (not apo-CIB1) would be the major form of the protein in a resting cell ([Mg^{2+}] $\sim 10^{-3}-10^{-4}$ M, [Ca^{2+}] $\sim 10^{-7}-10^{-8}$ M), and Ca^{2+} could bind to EF-III and EF-IV depending

† This research is supported by the Canadian Institutes of Health Research (CIHR). H.J.V. holds a senior scientist award from the Alberta Heritage Foundation for Medical Research (AHFMR). The NMR and biophysical equipment was purchased with funds provided by Canada Foundation for Innovation and the Alberta Science Research Authority. The biophysical equipment is operated through a Canada Foundation for Innovation Infrastructure Operating Fund grant. The Bio-NMR center at the University of Calgary is maintained through funds provided by the CIHR and the University of Calgary.

* Corresponding author. Phone: (403) 220-6006. Fax: (403) 289-9311. E-mail: vogel@ucalgary.ca.

‡ University of Calgary.

§ National Institute for Medical Research. Tel: (44)-20-8816-2100. Fax: (44)-20-8906-4477.

[1] Abbreviations: CIB1, calcium- and integrin-binding protein 1; CaM, calmodulin; NMR, nuclear magnetic resonance; TROSY, transverse relaxation optimized spectroscopy; WASS, weighted average secondary shift; CSP, chemical shift perturbation; LEM, linear extrapolation model; CD, circular dichroism; TnC, troponin C.

10.1021/bi700200z CCC: $37.00
Published on Web 05/22/2007

on the strength of the Ca^{2+} signal in a stimulated cell ([Mg^{2+}] $\sim 10^{-3}-10^{-4}$ M, [Ca^{2+}] $\leq 10^{-5}$ M). Both Mg^{2+}-CIB1 and Ca^{2+}-CIB1 can also bind to target proteins with high affinity, suggesting that each form of the protein may play a biological role in cell signaling (*8*).

Due to the importance of intracellular Ca^{2+} signaling in biology, the majority of EF-hand protein research has historically focused on characterization of the Ca^{2+}-bound forms. These forms also typically have more stable structures and more favorable spectral characteristics due to the tightly bound Ca^{2+} ions, making them more suitable for biophysical studies. Comparatively little is known about the apo- and Mg^{2+}-bound forms of EF-hand proteins, since they frequently have inferior spectral properties due to their less stable and more flexible structures, which often include molten globule-like apo-states (*9*−*14*). Since several EF-hand proteins in addition to CIB1 have been shown to bind Mg^{2+} (*12*, *14*−*16*) and interact with target proteins in a Ca^{2+}-independent manner (*13*, *17*, *18*), a better understanding of the structure and interactions of the apo- and Mg^{2+}-bound forms of these proteins is clearly required. The goal of the present study was to characterize the structure and stability of apo-CIB1 and Mg^{2+}-CIB1 in comparison to Ca^{2+}-CIB1, to obtain a better understanding of the unique Mg^{2+}- or Ca^{2+}-induced folding of the four EF-hand domains. Nuclear magnetic resonance (NMR) spectroscopy studies of apo-CIB1 and Mg^{2+}-CIB1 were first employed to obtain residue-specific information on the structure and metal-induced conformational changes in CIB1. We then replaced bulky hydrophobic amino acids in each EF-hand individually with Trp residues to provide site-specific spectroscopic probes that were used to monitor the EF-hand structure and stability under different conditions using steady-state fluorescence spectroscopy and chemical denaturation experiments. Wild type CIB1 contains no Trp residues, facilitating this approach. The NMR and fluorescence data are collectively used to generate a model describing the structure, stability, and metal-induced folding of CIB1.

EXPERIMENTAL PROCEDURES

Protein Expression, Purification, and Cloning. Unlabeled CIB1, ^{15}N-CIB1, and (perdeuterated) ^{2}H,^{13}C,^{15}N-CIB1 were expressed and purified to homogeneity as previously described (*3*, *4*). All single-Trp mutants of CIB1 (F34W, F91W, L128W, and F173W) were generated using the QuikChange site-directed mutagenesis kit (Stratagene), the CIB1-pET19b plasmid as a template (*4*), and the primers listed in Supplementary Table 1 (Supporting Information). The presence of each mutation was confirmed by DNA sequencing, and the mutant proteins (unlabeled and uniformly ^{15}N-labeled) were expressed and purified identically to wild type CIB1. Protein concentrations were determined using the predicted molar extinction coefficients for wild type CIB1 ($\epsilon_{276} = 2900\ M^{-1}\ cm^{-1}$) or Trp mutants ($\epsilon_{280} = 8250\ M^{-1}\ cm^{-1}$).

NMR Spectroscopy. NMR spectra were acquired on a Bruker AVANCE 700 MHz NMR spectrometer equipped with a triple resonance inverse cryoprobe with single axis *z*-gradient. Triple resonance NMR spectra were recorded at 37 °C using samples of 650 μM ^{2}H,^{13}C,^{15}N-CIB1, and the ^{1}H,^{15}N HSQC and {^{1}H}−^{15}N NOE experiments were performed using samples of 600 μM ^{15}N-CIB1. The buffer for all NMR experiments consisted of 20 mM HEPES, 100 mM KCl, 10 mM d_{10}-dithiothreitol, 10% D_2O, ~0.5 mM NaN_3, pH 7.5 ± 0.1, with an additional 2 mM EDTA and 2 mM EGTA for apo-CIB1 samples, 6 mM $MgCl_2$ and 1 mM EGTA for Mg^{2+}-CIB1 samples, and 3 mM $CaCl_2$ for Ca^{2+}-CIB1 samples. The small amount of high affinity Ca^{2+}-specific chelator EGTA in the Mg^{2+}-CIB1 samples is necessary and sufficient to remove bound Ca^{2+} from the protein, while the EDTA/EGTA in the apo-CIB1 samples sequesters both Mg^{2+} and Ca^{2+} (*4*).

All triple resonance (transverse relaxation optimized spectroscopy (TROSY)-based HNCACB, HN(CA)CO, HN(CO)CACB, and HNCO) and {^{1}H}−^{15}N NOE experiments were recorded and processed as previously described for Ca^{2+}-CIB1 (*3*). Analysis of the secondary structure for Mg^{2+}-CIB1 and the chemical shift differences between Mg^{2+}-CIB1 and Ca^{2+}-CIB1 were also performed as previously described using the weighted average secondary shift (WASS) and chemical shift perturbation (CSP) methods, respectively (*3*).

Steady-State Fluorescence Spectroscopy and Quenching. All fluorescence spectroscopy experiments were performed at room temperature on a Varian Cary Eclipse spectrofluorimeter, using samples of 10 μM wild type or Trp mutant CIB1 proteins in 50 mM HEPES, 100 mM KCl, 5 mM DTT, pH 7.5. Samples were supplemented with 1 mM EDTA and 1 mM EGTA for apo-CIB1 samples, 2 mM $MgCl_2$ and 0.5 mM EGTA for Mg^{2+}-CIB1 samples, and 1 mM $CaCl_2$ for Ca^{2+}-CIB1 samples. In all experiments the single Trp residue of the CIB1 mutants was selectively excited at 295 nm to avoid interference from the two endogenous Tyr residues (Y16 and Y110) of CIB1. The excitation and emission slits were set to 5 and 10 nm, respectively. Steady-state fluorescence emission spectra were recorded from 300 to 450 nm at a scan rate of 600 nm/min, and all of the presented spectra are the average of 3 scans with spectral smoothing performed using the Savitzky Golay algorithm provided in the Cary software.

Steady-state fluorescence quenching experiments were performed by titrating microliter volumes of 4 M acrylamide into 1 mL protein samples, and recording the steady-state fluorescence emission spectrum from 315 to 360 nm at each titration point. No shifting of the emission wavelength maximum (λ_{max}) was observed for any of the mutants suggesting that acrylamide does not alter the protein structure (data not shown). Therefore, the data were fit to the Stern−Volmer equation:

$$FI_0/FI = 1 + K_{SV}[Q] \quad (1)$$

where FI_0 and FI are the fluorescence intensity at λ_{max} in the absence and presence of acrylamide respectively, and [Q] is the quencher (acrylamide) concentration. All plots were linear, and the Stern−Volmer quenching constants (K_{SV}) were calculated by linear regression analysis. The quenching data represents the average and standard deviation of three independent experiments. The Trp amino acid (Trp) (purchased from Sigma) and the 26 amino acid αIIb-L peptide (αIIb-L), which has a single Trp residue in its sequence (Ac-LVLAM**W**KVGFFKRNRPPLEEDDEEGQ, purchased from AnaSpec, San Jose, CA), were also used as controls for the steady-state fluorescence quenching experiments.

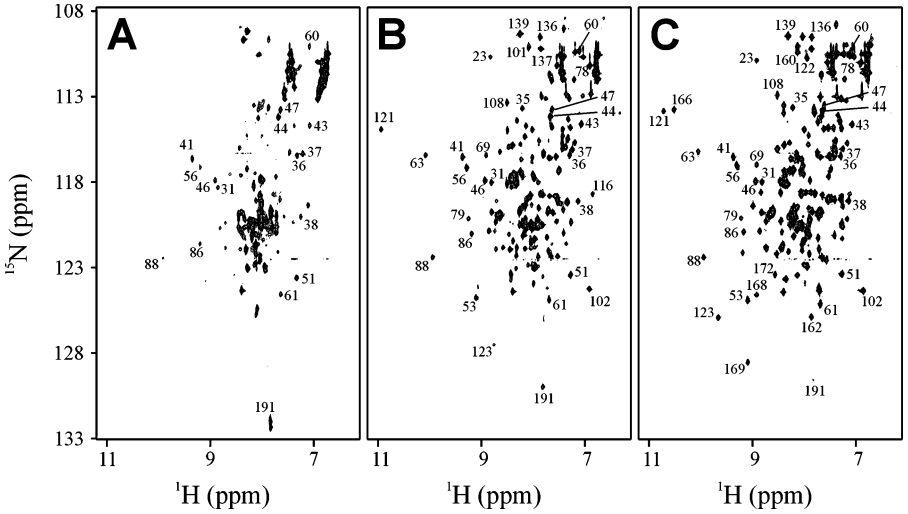

FIGURE 1: NMR fingerprint of the CIB1 protein backbone. ^{1}H,^{15}N HSQC NMR spectra of uniformly ^{15}N-labeled (A) apo-CIB1, (B) Mg^{2+}-CIB1, and (C) Ca^{2+}-CIB1. Each spectrum was recorded at 37 °C and pH 7.5, at a field strength of 700 MHz. Spectral assignments for Ca^{2+}-CIB1 (panel C) are taken from ref *3* while those for Mg^{2+}-CIB1 (panel B) are determined in the present study. Only the most dispersed peaks are labeled for clarity. The labeled residues in the apo-CIB1 spectrum (panel A) are extrapolated assignments based on the presence of similar or identical peaks in panels B and C.

Chemical Denaturation Experiments. Chemical denaturation experiments were performed by mixing samples of 10 μM protein in 0 M urea and 9 M urea, to obtain various intermediate final urea concentrations. Samples were incubated at room temperature for 4 h, and then steady-state fluorescence emission spectra were recorded at 20 °C using the steady-state fluorescence emission spectral parameters described above. The fluorescence signal at the λ_{max} of the native folded conformation ($\lambda_{max,N}$) was fitted using in-house software to either a two-state model describing a single transition between native (N) and unfolded (U) conformations (N $\rightarrow$ U) as previously described (*19*), eq 2,

$$Y = (I_N + S_N[D])f_N + (I_U + S_U[D])f_U \quad (2)$$

or a three-state model which includes an intermediate (I) conformation (N $\rightarrow$ I $\rightarrow$ U), eq 3, where $I_N/I_I/I_U$, $S_N/S_I/S_U$,

$$Y = (I_N + S_N[D])f_N + (I_I + S_I[D])f_I + (I_U + S_U[D])f_U \quad (3)$$

and $f_N/f_I/f_U$, are the intercept, slope, and fractional population values for the native/intermediate/unfolded forms of the protein, and [D] is the denaturant (urea) concentration. In eq 2 the fractional populations are calculated as $f_U = K_U/(1 + K_U)$ and $f_N = 1.0 - f_U$, where $K_U = \exp(-\Delta G_U/RT)$ and ΔG_U is calculated using the linear extrapolation model (LEM), eq 4 (*20*),

$$\Delta G_U = \Delta G^\circ + \mathbf{m}[D] \quad (4)$$

where ΔG° is the standard free energy of unfolding in the absence of denaturant, and **m** is the dependence of ΔG_U on [D]. In eq 3 the fractional populations are calculated as $f_N = 1/(1 + K_{NI} + K_{NI}K_{IU})$, $f_I = K_{NI}/(1 + K_{NI} + K_{NI}K_{IU})$, and $f_U = K_{NI}K_{IU}/(1 + K_{NI} + K_{NI}K_{IU})$, where $K_{NI} = \exp(-\Delta G_{NI}/RT)$ and $K_{IU} = \exp(-\Delta G_{IU}/RT)$. The ΔG_{NI} and ΔG_{IU} values are calculated as $\Delta G_{NI} = \Delta G^\circ_{NI} + \mathbf{m}_{NI}[D]$ and $\Delta G_{IU} = \Delta G^\circ_{IU} + \mathbf{m}_{IU}[D]$. The denaturant concentration at the midpoint of each transition (C_m) was also calculated as $\Delta G^\circ/\mathbf{m}$.

RESULTS

Backbone Structure and Flexibility of CIB1 Probed by NMR Spectroscopy. ^{1}H,^{15}N HSQC NMR spectra of CIB1 provide a useful fingerprint of the protein structure since each peak represents one backbone or side chain amide group. The HSQC spectrum of Ca^{2+}-CIB1 exhibits good peak dispersion and narrow line width typical for a folded and stable structure, Figure 1C. These favorable spectral properties facilitated nearly complete backbone resonance assignment of the protein using (perdeuterated) ^{2}H,^{13}C,^{15}N-CIB1 and TROSY-based triple resonance NMR spectroscopy experiments as previously described (*3*). Although somewhat fewer HSQC peaks are detected in the presence of Mg^{2+}, the quality of the triple resonance NMR data for Mg^{2+}-CIB1 was also suitable to obtain backbone resonance assignments using ^{2}H,^{13}C,^{15}N-CIB1 and TROSY-based NMR pulse sequences, Figure 1B. In contrast, the HSQC spectrum of apo-CIB1 contains only a small number of dispersed resonances characteristic of folded protein regions, has a significant number of resonances with typical random coil chemical shifts ($\sim$7.5 $-$ 8.5 ppm in the ^{1}H dimension), and has many resonances broadened completely beyond detection by chemical exchange, Figure 1A. The poor spectral quality for apo-CIB1 could not be improved under different solution or experimental conditions including at lower protein concentrations, suggesting that protein aggregation was not responsible for the resonance line broadening (data not shown). Apo-CIB1 has also been shown to be monomeric in solution using several techniques (*7*, *21*, *22*). On the other hand, a lack of long-range NOE's in homonuclear ^{1}H$-^{1}$H NOESY NMR spectra of apo-CIB1 is suggestive of a dynamic structure for the metal-free protein, Supplementary Figure 1 (Supporting Information). Unfortunately this chemical exchange made it impossible to obtain the spectral assignments for apo-CIB1 from triple resonance NMR data. Interestingly however, some of the well-resolved apo-CIB1 HSQC peak assignments could be inferred based on similar or identical peaks in the Mg^{2+}-CIB1 and Ca^{2+}-CIB1 spectra,

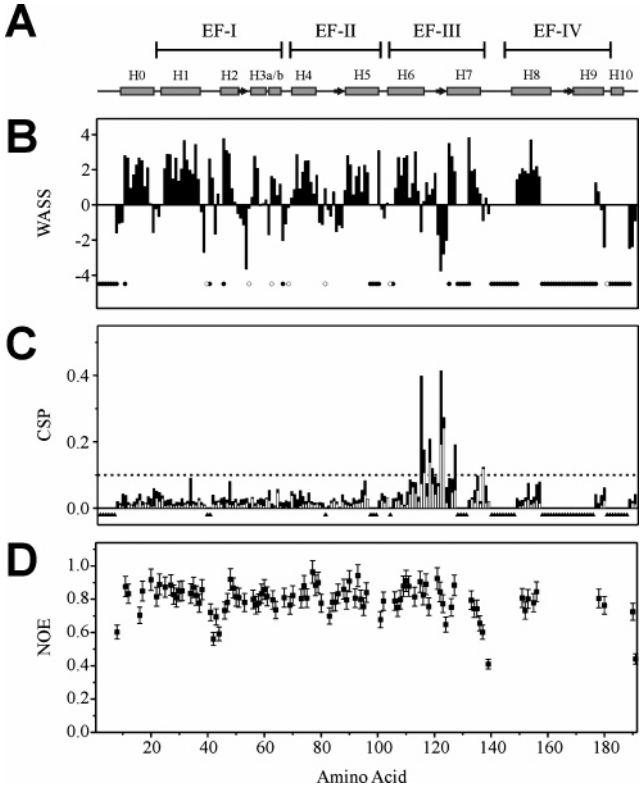

FIGURE 2: Backbone structure and flexibility of Mg^{2+}-CIB1, and comparison to Ca^{2+}-CIB1. (A) Schematic diagram showing the secondary structure of Ca^{2+}-CIB1 (*3*), with α-helices H0−H10 and *β*-strands represented by boxes and arrows, respectively. (B) Weighted average secondary shift (WASS) values are used to predict the secondary structure of Mg^{2+}-CIB1 in solution, where positive WASS values are characteristic of α-helices, and negative WASS values are characteristic of *β*-strands and other extended conformations. Solid circles in the lower part of the panel indicate residues for which the backbone amide resonances could not be assigned in the triple resonance NMR data, and open circles show the location of proline residues. (C) Chemical shift perturbation (CSP) values reveal the residue-specific chemical shift differences between Mg^{2+}-CIB1 and Ca^{2+}-CIB1. The CSP contributions from HN and N nuclei are shown together as open bars, and the contributions from Cα and C*β* nuclei are shown together as solid bars. The dotted horizontal line indicates an arbitrary CSP cutoff value of 0.1. Residues that could not be analyzed in the CSP data are indicated by up-triangles in the lower part of the panel. (D) $\{^1H\}-^{15}N$ NOE data for Mg^{2+}-CIB1 provide information on the backbone flexibility of the protein in solution.

and all of these dispersed peaks correspond to residues in EF-I or the loop region of EF-II (L86, F88) which interacts with EF-I in the crystal structure of Ca^{2+}-CIB1 (*7*). This implies that this N-terminal region of apo-CIB1 adopts a somewhat more stable fold than EF-II, EF-III, and EF-IV, and retains a similar structure in the presence of Mg^{2+} or Ca^{2+}. The stability and structural integrity of this EF-I region under all three conditions (apo-, Mg^{2+}-bound, and Ca^{2+}-bound) was also evident from fluorescence spectroscopy experiments (see below).

The NMR chemical shift data for Mg^{2+}-CIB1 is summarized and compared to the data for Ca^{2+}-CIB1 in Figure 2. The secondary structure of Mg^{2+}-CIB1 was predicted using the weighted average secondary shift (WASS) method (Figure 2B), conformational differences between Mg^{2+}-CIB1 and Ca^{2+}-CIB1 were examined using chemical shift perturbation (CSP) (Figure 2C), and the backbone flexibility of Mg^{2+}-CIB1 was investigated by $\{^1H\}-^{15}N$ NOE experiments, Figure 2D. These analyses reveal a nearly identical secondary structure and very small CSP values for the N-lobe of Mg^{2+}-CIB1 in comparison to Ca^{2+}-CIB1, indicating that the N-lobe adopts essentially the same backbone fold in the presence of Mg^{2+} or Ca^{2+}. Also like Ca^{2+}-CIB1, the $\{^1H\}-^{15}N$ NOE values for the N-lobe of Mg^{2+}-CIB1 are generally ∼0.8, which is typical for a stable folded structure, and the loop connecting α-helix 1 (H1) to H2 exhibits slightly increased flexibility ($\{^1H\}-^{15}N$ NOE values ∼0.6), Figure 2D. The glycine-rich extreme N-terminus of CIB1 is predicted to be highly flexible (*7*), and the peaks corresponding to this region are not observable for either Mg^{2+}-CIB1 (Figure 2B) or Ca^{2+}-CIB1 (*3*) presumably because of the rapid amide hydrogen exchange that occurs with solvent water under these conditions of high temperature (37 °C) and pH (7.5).

Unlike the N-lobe, we found significant differences in the NMR chemical shift data for the C-lobe of Mg^{2+}-CIB1 in comparison to Ca^{2+}-CIB1. The most notable difference is that nearly 50% of the C-lobe NMR signals are severely broadened by chemical exchange and cannot be assigned in the triple resonance NMR data for Mg^{2+}-CIB1, Figure 2B. The C-lobe residues that could be unambiguously assigned include most of EF-III, the central portion of α-helix H8 from EF-IV (K150−L157), and the unique S178-R179-S180 tripeptide sequence in the loop connecting EF-IV to the C-terminal extension. The dipeptide sequences E126-D127 at the C-terminal end of the EF-III metal-binding loop and V190-L191 at the extreme C-terminus of the protein could also be assigned based on their distinct chemical shifts and the assigned spectra of Ca^{2+}-CIB1. The regions of the Mg^{2+}-CIB1 C-lobe that could not be assigned include the central portion of α-helix H7 (EF-III), the entire metal-binding loop and exiting α-helix (H9) of EF-IV, and most of the C-terminal extension. We note that a small number of additional very weak signals, likely corresponding to some of these exchanged-broadened C-lobe regions, were observed in the Mg^{2+}-CIB1 HSQC spectrum, but these HSQC peaks did not give rise to detectable signals in the triple resonance data due to the much lower sensitivity of triple resonance NMR spectroscopy experiments. The Mg^{2+}-CIB1 spectra were also not significantly improved under different conditions such as at higher or lower temperatures or in the presence of a large Mg^{2+} excess (50 mM $MgCl_2$) (data not shown). The peak broadening for these regions of Mg^{2+}-CIB1 suggest that they retain some of the exchange properties of apo-CIB1.

For the assignable Mg^{2+}-CIB1 C-lobe residues, the WASS analysis reveals an identical secondary structure to Ca^{2+}-CIB1, Figure 2. The CSP values for these C-lobe residues were generally larger than for the N-lobe residues, but were quite small when compared, for example, to the shifts induced by target peptide binding to CIB1. More specifically, only 8 residues have CSP values greater than 0.1 when comparing the NMR data for Mg^{2+}-CIB1 to Ca^{2+}-CIB1 (Figure 2C), whereas 51 residues have CSP values greater than 0.1 when comparing Ca^{2+}-CIB1 alone and in complex with a target peptide (*3*). Not surprisingly, all of the residues with large CSP values in Figure 2C are found in the Ca^{2+}-and-Mg^{2+}-binding EF-hand, EF-III, and more specifically localized to the actual Ca^{2+}/Mg^{2+}-binding loop of EF-III. Therefore the larger chemical shift differences for these

Table 1: Steady-state Fluorescence Spectroscopy Data for Trp Mutants of CIB1

sample	λ_{max} (nm)	K_{SV}[a] (M^{-1})
Trp	355	20.7 ± 0.3
peptide Trp[b]	355	14.8 ± 1.5
apo-F34W	321	1.2 ± 0.2
Mg^{2+}-F34W	318	1.1 ± 0.2
Ca^{2+}-F34W	318	1.2 ± 0.1
apo-F91W	325	1.8 ± 0.1
Mg^{2+}-F91W	324	2.2 ± 0.2
Ca^{2+}-F91W	325	2.5 ± 0.2
apo-L128W	334	4.1 ± 0.1
Mg^{2+}-L128W	327	2.3 ± 0.1
Ca^{2+}-L128W	320	2.0 ± 0.1
apo-F173W	331	3.1 ± 0.1
Mg^{2+}-F173W	326	1.9 ± 0.2
Ca^{2+}-F173W	326	1.6 ± 0.1

[a] K_{SV} values represent the average and standard deviation of 3 independent measurements. [b] The peptide sequence is as follows: Ac-LVLAM**W**KVGFFKRNRPPLEEDDEEGQ, where Ac symbolizes an acylated N-terminus.

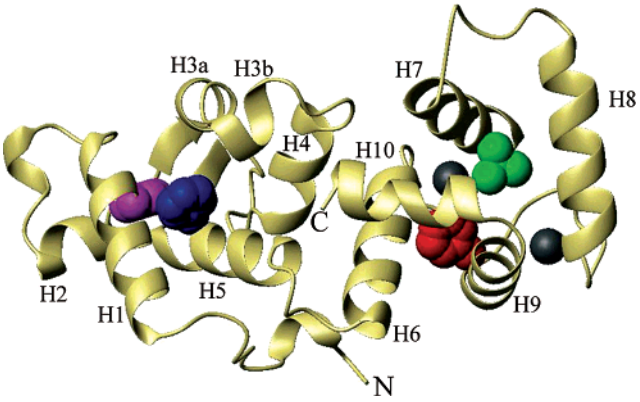

FIGURE 3: Structure of Ca^{2+}-CIB1 (PDB: 1XO5) illustrating the location of the four residues that were individually mutated to Trp in this study: F34 (magenta), F91 (blue), L128 (green), F173 (red). The α-helices H1−H10 as well as the N- and C-termini are labeled. Note that H0 is not observed in this crystal form of Ca^{2+}-CIB1, but is present in solution (*3*). Ca^{2+} ions bound to EF-III and EF-IV in the C-lobe are represented by black spheres.

residues are probably induced by the unique chemistry of the Mg^{2+} or Ca^{2+} ions coordinated by EF-III, rather than being due to a large structural change in this region of the protein. Importantly, the $\{^1H\}-^{15}N$ NOE values for the C-lobe of Mg^{2+}-CIB1, including the assignable EF-IV residues, are generally near ~0.8, suggesting that the fourth EF-hand does not completely unfold in the absence of a bound metal ion at this site, Figure 2D. Of the residues that could be analyzed in the $\{^1H\}-^{15}N$ NOE data, only G137 and G139 in the loop connecting EF-III to EF-IV and L191 at the extreme C-terminus had $\{^1H\}-^{15}N$ NOE values ≤0.6, and both of these regions also have elevated flexibility in the Ca^{2+}-bound protein (*3*). Therefore, the NMR data collectively suggest that the C-lobe of Mg^{2+}-CIB1 adopts a similar secondary structure and global fold to Ca^{2+}-CIB1, and that the unassignable regions may be in exchange between multiple conformations, but are not completely unfolded.

Steady-State Fluorescence Spectroscopy and Quenching of Trp Substituted CIB1 Proteins. To compliment our NMR spectroscopy data, we used fluorescence spectroscopy as an additional approach to investigate the structure and stability of apo-CIB1, Mg^{2+}-CIB1, and Ca^{2+}-CIB1. Because wild type CIB1 contains no Trp residues, we generated 4 mutant CIB1 proteins each with a single Trp reporter group in one of the four EF-hands. The four mutants are as follows: F34W (EF-I), F91W (EF-II), L128W (EF-III), and F173W (EF-IV), with each substitution replacing a bulky hydrophobic residue with Trp. In the crystal structure of Ca^{2+}-CIB1 (*7*), F34 is located deep within the interior of the N-lobe at the C-terminal end of H1, and has its side chain sandwiched between H2 and the N-terminal portion of H5, Figure 3. The F91 side chain is closer to the surface of the protein than F34, but is also shielded from the solvent by the side chains of L37 (H1) and L61 (H3b). The L128 and F173 side chains are on the hydrophobic face of H7 (EF-III) and H9 (EF-IV), respectively, with the L128 side chain interacting with the central region of H8, and the F173 side chain interacting with the central part of H6. In the structure of Ca^{2+}-CIB1 both the L128 and F173 side chains are buried by the C-terminal extension, Figure 3. Thus in the Ca^{2+}-bound form of CIB1 each of the four Trp-substituted residues is completely buried, with less than 0.5% of the side chain surface area accessible to the solvent as calculated using the predictive program GetArea 1.1 (*23*). Far-UV circular dichroism (CD) spectra and $^1H,^{15}N$ HSQC NMR spectra of each mutant in the presence or absence of Mg^{2+} or Ca^{2+} reveal that none of the Trp substitutions significantly perturb the structure of the protein, making them suitable reporter groups for structural and stability studies, Supplementary Figures 2 and 3 (Supporting Information).

The Mg^{2+}- and Ca^{2+}-induced conformational changes in the microenvironment of each Trp residue were first examined using steady-state fluorescence spectroscopy and acrylamide quenching experiments. The data is summarized in Figure 4 and Table 1. The free Trp amino acid and the single Trp residue of a 26 amino acid random coil peptide (αIIb-L) were used as controls, with free Trp representing a fully solvent exposed Trp residue, and the Trp of the αIIb-L peptide representing the Trp microenvironment within an unstructured polypeptide chain. Note that the far-UV CD spectrum of the αIIb-L peptide under similar conditions is characteristic of a completely random coil structure (data not shown).

The steady-state fluorescence emission wavelength maximum (λ_{max}) for apo-F34W is significantly blue-shifted (λ_{max} = 321 nm) in comparison to the Trp controls (λ_{max} = 355 nm), suggesting that the W34 residue is in a nonpolar chemical environment, Figure 4A, Table 1. The K_{SV} value for apo-F34W (K_{SV} = 1.2 ± 0.2 M^{-1}) is also very small, consistent with the burial of W34 deep within the interior of the N-lobe. Only minor changes in the fluorescence intensity, λ_{max}, and K_{SV} values are observed upon addition of either Mg^{2+} or Ca^{2+} to apo-F34W, suggesting that neither metal induces substantial conformational changes in the microenvironment surrounding the W34 side chain. Therefore the region surrounding W34 in EF-I of apo-F34W appears to be well-folded and maintain a similar structure upon Mg^{2+}- or Ca^{2+}-binding to the mutant, consistent with the folded EF-I structure implied by the NMR data, Figure 1. The λ_{max} (324−325 nm) and K_{SV} (1.8−2.5 M^{-1}) values for F91W are slightly larger than for F34W, but are still typical for a buried Trp residue, Figure 4B, Table 1. However, with F91W there is a small increase in the K_{SV} values and there are obvious

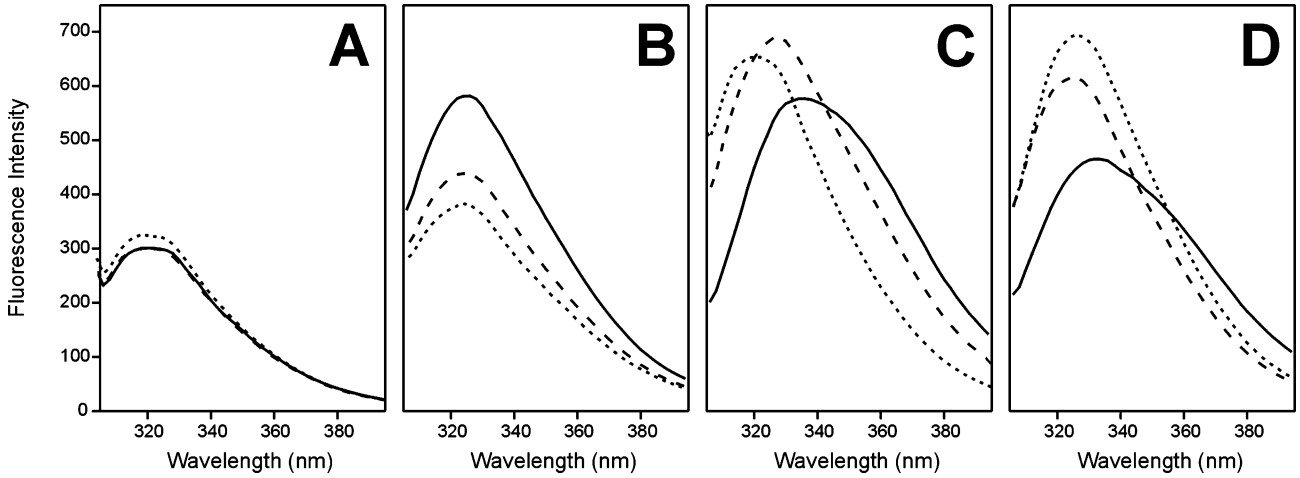

FIGURE 4: Mg^{2+}- and Ca^{2+}-induced conformational changes in the Trp mircoenvironment of CIB1 Trp mutants. Steady-state fluorescence emission spectra of (A) F34W, (B) F91W, (C) L128W, and (D) F173W, with the apo-, Mg^{2+}-bound, and Ca^{2+}-bound forms of each protein represented by solid, dashed, and dotted lines, respectively. The fluorescence intensity on the *y*-axis is shown in arbitrary units.

changes in fluorescence intensity upon addition of Mg^{2+} or Ca^{2+} to the apoprotein, implying that the region surrounding W91 undergoes conformational changes upon metal-binding. Since Mg^{2+} and Ca^{2+} bind only to the C-lobe of CIB1, the fluorescence changes for the W91 reporter group in the N-lobe indicate that the two lobes of the protein are in close association and communicate Mg^{2+}- or Ca^{2+}-induced conformational changes between them.

In the absence of Mg^{2+} or Ca^{2+}, the λ_{max} values for the C-lobe mutants apo-L128W (334 nm) and apo-F173W (331 nm) are at longer wavelengths than the N-lobe mutants, and the corresponding K_{SV} values are somewhat larger ($K_{SV} = 4.1 \pm 0.1\ M^{-1}$ and $3.1 \pm 0.1\ M^{-1}$, respectively), Figure 4C,D, Table 1. This indicates that the Trp residues of L128W and F173W in the metal-free C-lobe are slightly more solvent exposed than those of the N-lobe, although still much less exposed to the solvent than the Trp or αIIb-L peptide controls. Upon Mg^{2+}- or Ca^{2+}-binding to L128W or F173W, the λ_{max} values shift to shorter wavelengths, the K_{SV} values decrease, and there are distinct changes in the fluorescence intensity. Therefore, the binding of either metal induces conformational changes in the C-lobe that result in W128 (L128W) and W173 (F173W) becoming less exposed to the solvent.

Chemical Denaturation of Trp Mutants. The stability of CIB1 was next examined by performing urea-induced denaturation experiments using the four Trp mutants of CIB1. As expected, increasing urea concentrations shift the λ_{max} values for each Trp mutant from those characteristic of the native (N) state ($\lambda_{max,N}$, Table 1) to ~355 nm for the unfolded (U) state ($\lambda_{max,U}$), as the Trp residues become exposed to the polar solvent in the denatured protein, for example see Figure 5A,B. The changes in fluorescence intensity at $\lambda_{max,N}$ were fit using the linear extrapolation model (LEM) (*20*) to estimate the standard free energy of unfolding in the absence of denaturant ($\Delta G°$), the dependence of $\Delta G°$ on the denaturant concentration (**m**), and the unfolding transition midpoint (C_m). A summary of the LEM analysis is presented in Table 2. Of these values the C_m is generally considered to be the most accurate representation of protein stability and will be discussed in the most detail below, whereas $\Delta G°$ and **m** are highly correlated and more sensitive to small fluctuations in the experimental data (*24*, *25*).

Interestingly, the denaturation profiles for each mutant protein reveal different unfolding behavior and distinct effects of Mg^{2+} and Ca^{2+} on the stability of the various regions of CIB1, Figure 5. Denaturation as monitored by apo-F34W reveals a distinct one-step two-state N → U transition spanning ~3 − 5 M urea, with $C_m = 4.1$ M, $\Delta G° = 5.4 \pm 0.2$ kcal/mol, $\mathbf{m} = -1.3$ kcal/mol/M, and well-defined pre- and post-transition baselines, Figure 5C, Table 2. These values are comparable to other EF-hand proteins of similar size (*11*, *12*, *26*), confirming that the region surrounding W34 in F34W is well-folded and stable even in the absence of Mg^{2+} or Ca^{2+}. A similar unfolding curve is obtained for F34W in the presence of Mg^{2+} ($C_m = 4.2 \pm 0.1$ M), but a small increase in stability is observed in the presence of Ca^{2+} ($C_m = 5.0 \pm 0.2$ M). Therefore, although Ca^{2+} binding to the C-lobe does not induce a large conformational change surrounding W34 (Figure 4A), it does marginally increase the N-lobe stability, providing additional evidence for interlobe communication in CIB1.

At the other end of the protein, the F173W denaturation data is also best described by a one step N → U transition, Figure 5A,F. However there is a much larger influence of Mg^{2+} and Ca^{2+} on the unfolding behavior than seen with F34W. The immediate decrease in the fluorescence intensity for apo-F173W at very low [urea] suggests that the region surrounding the W173 residue in EF-IV of F173W is very unstable, and is in fact partially unfolded even without urea present. The broadness of the transition also implies that the unfolding of this region might proceed through one or more intermediate conformational states. Unfortunately, the absence of a pre-transition baseline or clear inflection point precluded the extraction of the unfolding thermodynamic values for apo-F173W. However, pretransition baselines and inflection points are well-defined for both Mg^{2+}-F173W and Ca^{2+}-F173W, and LEM analysis shows that each metal can stabilize the structure surrounding W173 of this mutant, with Ca^{2+} ($C_m = 6.0 \pm 0.1$ M) having a significantly larger stabilizing effect than Mg^{2+} ($C_m = 3.0 \pm 0.1$ M). Importantly, the non-coincidence of the unfolding transitions for F34W in comparison to F173W suggests that these two distinct regions at either end of the protein do not unfold in a cooperative manner.

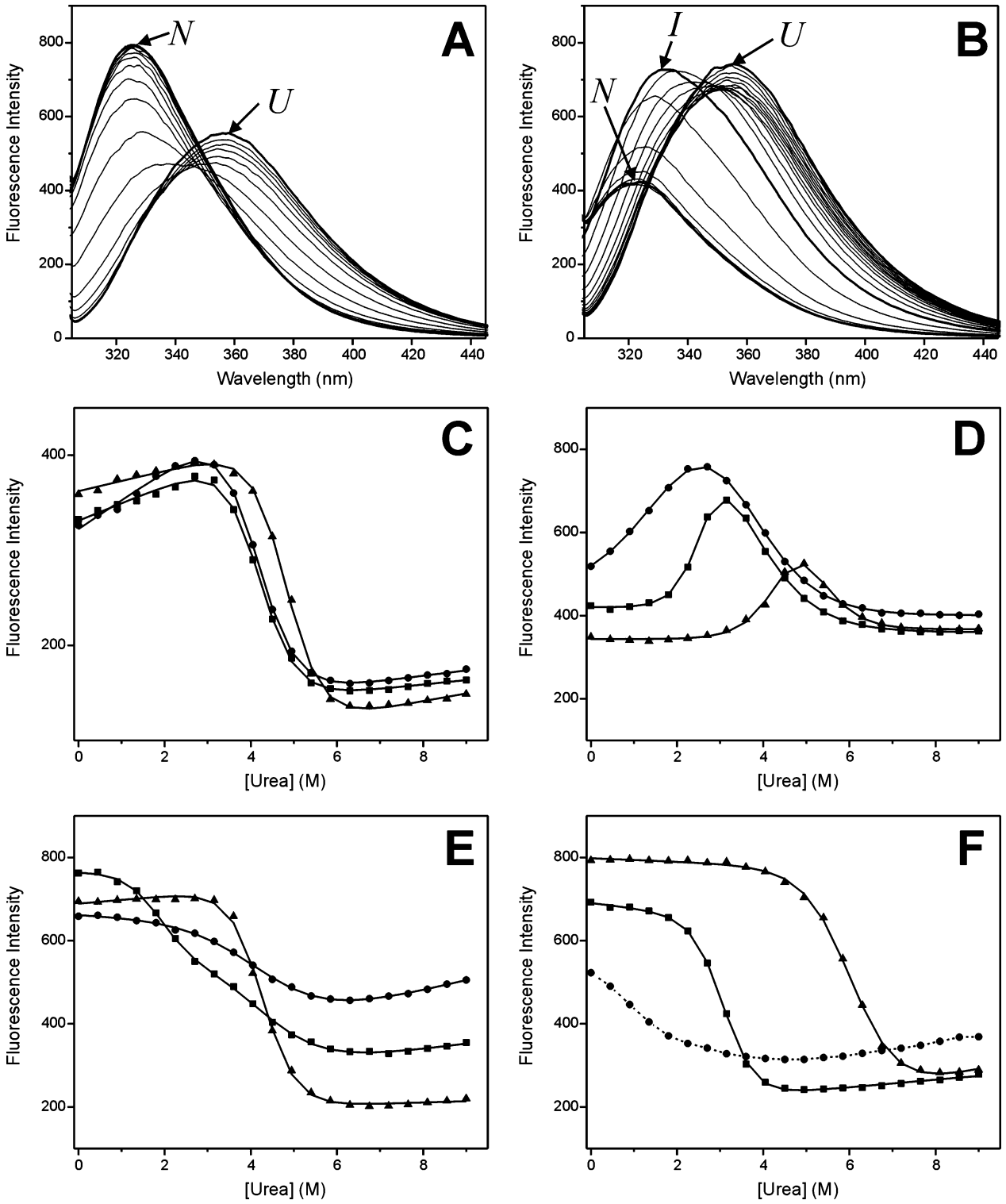

FIGURE 5: Chemical denaturation of CIB1 Trp mutants. Representative steady-state fluorescence emssion spectra for (A) Ca^{2+}-F173W and (B) Mg^{2+}-F91W at various concentrations of urea between 0 and 9 M. The native (N) and unfolded (U) forms of each protein at 0 M urea and 9 M urea respectively are shown in bold and labeled. In the case of Mg^{2+}-F91W, but not Ca^{2+}-F173W, an intermediate (I) conformation is also evident as indicated in panel B. The bottom four panels show representative denaturation profiles for (C) F34W, (D) F91W, (E) L128W, and (F) F173W in the apo-form (●), with Mg^{2+}-bound (■), or with Ca^{2+}-bound (▲). The solid lines represent the best fit to the data using the linear extrapolation model (LEM). LEM analysis of the apo-F173W data could not be performed, so the data points are jointed by a dotted line (see text for details). The unfolding was monitored by measuring the fluorescence intensity at $\lambda_{max,N}$, with the fluorescence intensity shown in arbitrary units.

In contrast to F34W and F173W, the unfolding behavior of CIB1 as monitored by the F91W (EF-II) and L128W (EF-III) mutants did not follow a simple N → U transition in most cases. This is most obvious in the data for F91W, where a distinct but transient, hyperfluorescent intermediate (I) is apparent for all three forms of the protein, Figure 5B,D. The λ_{max} values for the I conformation of apo-F91W ($\lambda_{max,I}$ ~328 nm), Mg^{2+}-F91W ($\lambda_{max,I}$ ~332 nm), and Ca^{2+}-F91W ($\lambda_{max,I}$ ~339 nm) are each red-shifted with respect to the N conformations, suggesting that the Trp residue becomes

Table 2: Urea-Induced Unfolding of CIB1 Trp Mutants as Determined by Fluorescence Spectroscopy[a]

condition	unfolding step[b]	$\Delta G°$ (kcal/mol)	**m** (kcal/mol/M)	C_m (M)
apo-F34W	N → U	5.4 ± 0.2	−1.3 ± 0.0	4.1 ± 0.0
Mg^{2+}-F34W	N → U	6.0 ± 0.5	−1.4 ± 0.1	4.2 ± 0.1
Ca^{2+}-F34W	N → U	7.5 ± 0.8	−1.5 ± 0.1	5.0 ± 0.2
apo-F91W	N → I	1.1 ± 0.2	−0.6 ± 0.0	1.7 ± 0.4
	I → U	2.6 ± 0.4	−0.8 ± 0.1	3.2 ± 0.4
Mg^{2+}-F91W	N → I	4.3 ± 0.5	−1.7 ± 0.2	2.6 ± 0.1
	I → U	2.8 ± 0.6	−0.8 ± 0.1	3.6 ± 0.1
Ca^{2+}-F91W	N → I	5.6 ± 0.3	−1.3 ± 0.1	4.5 ± 0.0
	I → U	6.7 ± 0.5	−1.3 ± 0.1	5.2 ± 0.1
apo-L128W	N → U	2.6 ± 0.4	−0.6 ± 0.1	4.1 ± 0.3
Mg^{2+}-L128W	N → I	2.6 ± 0.5	−1.5 ± 0.3	1.8 ± 0.1
	I → U	3.5 ± 0.1	−0.8 ± 0.1	4.2 ± 0.2
Ca^{2+}-L128W	N → U	6.2 ± 0.4	−1.4 ± 0.1	4.3 ± 0.2
apo-F173W[c]	N → U			
Mg^{2+}-F173W	N → U	4.5 ± 0.6	−1.5 ± 0.1	3.0 ± 0.1
Ca^{2+}-F173W	N → U	6.3 ± 0.2	−1.1 ± 0.0	6.0 ± 0.1

[a] All data represents the average and standard deviation of three independent experiments. [b] N, I, and U symbolize the native, intermediate, and unfolded conformations of CIB1, respectively. [c] Analysis of the apo-F173W data could not be performed (see text for details).

slightly more exposed to the solvent in the intermediate conformation. The formation of the apo-F91W intermediate (N → I) begins at 0 M urea and closely parallels the unfolding curve for apo-F173W. Meanwhile, the second (I → U) transition for apo-F91W occurs between ~3 and 5 M urea, similar to the unfolding curve for apo-F34W. Likewise the N → I and I → U transitions for Mg^{2+}-F91W closely coincide with the single N → U unfolding curves for Mg^{2+}-F173W and Mg^{2+}-F34W, respectively. This parallel unfolding behavior as monitored by Trp reporter groups in different regions of the protein implies that the denaturation of the F173 region in apo-CIB1 and Mg^{2+}-CIB1 results in an intermediate conformation in the F91 region, and at higher [urea] this intermediate unfolds together with the F34 region. Fitting these apo-F91W and Mg^{2+}-F91W denaturation data to a two-step three-state N → I → U model yields estimated thermodynamic values associated with each of the two unfolding steps, Table 2. Considering that the pretransition baseline slope and intercept values for the N and I (apo-F91W) and I (Mg^{2+}-F91W) conformations are undefined by the data and estimated during curve fitting, the C_m values obtained from the fit are in reasonable agreement with the hypothesized unfolding model described above, Table 2. Interestingly, two unfolding transitions are also observed for Ca^{2+}-F91W, but in this case the first and second transitions closely coincide with the unfolding curves of Ca^{2+}-F34W and Ca^{2+}-F173W, respectively, Figure 5. This suggests that, in the presence of Ca^{2+}, the unfolding of the F34 region results in the formation of an intermediate in the F91 region, and this intermediate completely unfolds together with the F173 region at higher [urea]. The value ($C_{m,N\rightarrow I}$ = 4.5 M) obtained from the LEM analysis of the Ca^{2+}-F91W data is in reasonable agreement with the value obtained for Ca^{2+}-F34W ($C_{m,N\rightarrow U}$ = 5.0 ± 0.2 M), but the value ($C_{m,I\rightarrow U}$ = 5.2 ± 0.1 M) for Ca^{2+}-F91W is somewhat lower than that for Ca^{2+}-F173W ($C_{m,N\rightarrow U}$ = 6.0 ± 0.1 M). This might indicate that the intermediate conformation in the F91 region unfolds just prior to the N → U transition in the F173 region of Ca^{2+}-CIB1. However, as with the I → U transitions of apo-F91W and Mg^{2+}-F91W, the $C_{m,I\rightarrow U}$ value for Ca^{2+}-F91W might be underestimated because of the poorly defined pretransition baseline region for the I → U unfolding step.

The chemical denaturation data for apo-L128W exhibited a single broad transition beginning between 0 and 1 M urea and was complete near ~6.5 M urea, with a C_m value of 4.1 M, Figure 5E, Table 2. Importantly, the **m** value for this broad transition (**m** = −0.6 kcal/mol/M) is very small compared to the single N → U transitions for F34W and F173W (**m** = −1.1 to −1.5 kcal/mol/M). This signifies the presence of an intermediate state(s) that cannot be resolved due to the similarity in the fluorescence spectra of the N, I, and U forms of the protein. The denaturation transition for Mg^{2+}-L128W also spanned a similar [urea] range of ~0 to 6.5 M urea, but the change in fluorescence intensity was larger than for apo-L128W, and consequently overlapping N → I and I → U transitions could be better resolved, Figure 5E. LEM analysis of the Mg^{2+}-L128W denaturation data suggests that the I → U transition ($C_{m,I\rightarrow U}$ = 4.2 ± 0.2 M) coincides with the unfolding of Mg^{2+}-F34W ($C_{m,N\rightarrow U}$ = 4.2 ± 0.1 M), but that the N → I transition for Mg^{2+}-L128W occurs at lower [urea] ($C_{m,N\rightarrow I}$ = 1.8 ± 0.1 M) than Mg^{2+}-F173W ($C_{m,N\rightarrow U}$ = 3.0 ± 0.1 M). Therefore, the region of Mg^{2+}-CIB1 surrounding residue 128 appears to be the least stable region of the protein, and may unfold just prior to the region surrounding residue 173. The denaturation data for Ca^{2+}-L128W displayed a single sharp transition with C_m = 4.3 M, which coincides with the single N → U transition of Ca^{2+}-F34W, and the N → I transition of Ca^{2+}-F91W.

DISCUSSION

Based on the structure of Ca^{2+}-CIB1 (*3*, *7*), the known metal binding characteristics of the protein (*4*), and the present structural and chemical denaturation data, we can devise a model for the Mg^{2+}- and Ca^{2+}-induced conformational changes in CIB1, as well as for the urea-induced unfolding pathway for each form of the protein, Figure 6. Apo-CIB1 has significant α-helical character and some tertiary structure, and the Trp reporter groups in each of the four EF-hand domains are considerably shielded from the solvent, indicating that the protein is predominantly folded in the absence of Mg^{2+} or Ca^{2+} (Table 1, Supplementary Figure 2) (*4*). However, the chemical exchange-broadened NMR spectra clearly show that the tertiary structure of apo-CIB1 is unstable (Figure 1, Supplementary Figure 1). Interestingly, the entire apo-CIB1 protein does not exhibit the same exchange behavior, but rather, the data suggest that a gradient of stability exists across the apo-CIB1 molecule. The N-terminal end of apo-CIB1, more specifically the F34 region of EF-I, appears to be the most stable region of the protein, and adopts a structure that is similar to the structure of this region in Mg^{2+}-CIB1 and Ca^{2+}-CIB1, Figure 6A. On the other hand, the F173 region at the C-terminal end of the protein is partially unfolded even in the absence of denaturant, and the intervening F91 and L128 regions are in exchange between multiple predominantly folded conformations. At low [urea] the F34 region remains structurally intact, while the F173 region completely unfolds and shifts the conformational equilibrium in the F91 and L128 regions toward a transient intermediate conformation. This intermediate structure in the F91 and L128 regions, and the native

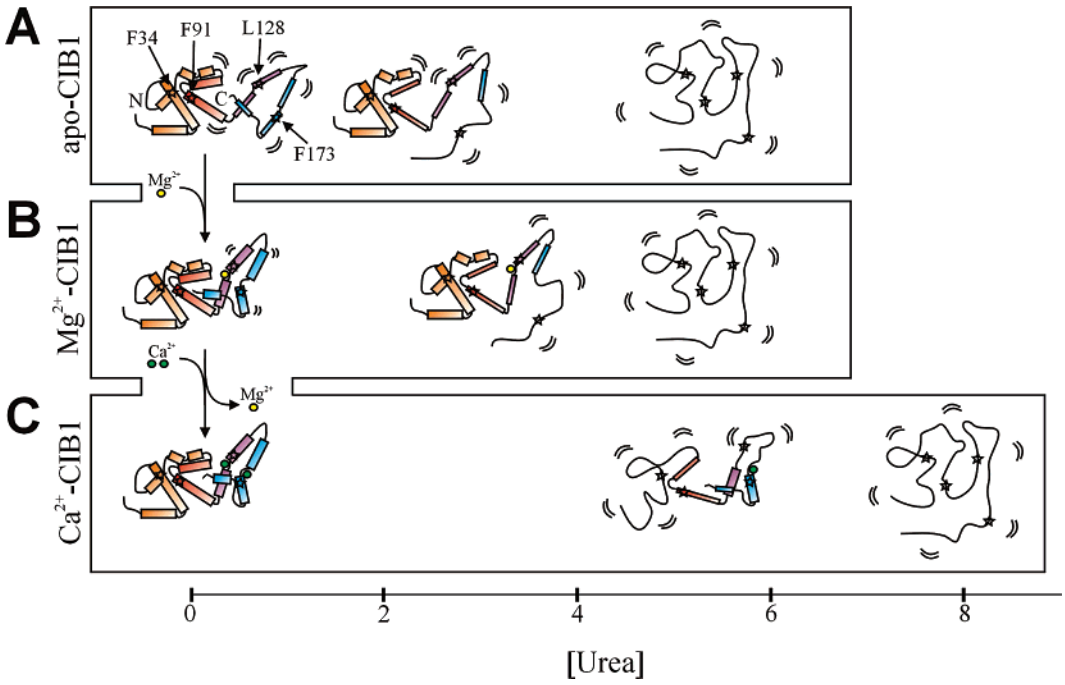

FIGURE 6: Schematic model for the urea-induced denaturation of CIB1. α-Helices are shown as boxes, with thicker boxes representing more structurally stable α-helices, and thinner boxes indicating partially unfolded or more flexible regions of the protein. The location of the four Trp-substituted residues (F34, F91, L128, and F173) are indicated by stars, and labeled in panel A. The four EF-hands are color coded in orange (N-terminal extension and EF-I), red (EF-II), purple (EF-III), and blue (EF-IV and C-terminal extension). The N- and C-termini are also labeled in panel A.

structure in the F34 region, ultimately unfold together near a urea concentration of ~5 M, Figure 6A.

Mg^{2+} binding to EF-III stabilizes the structure of CIB1, which significantly improves the NMR spectra (Figure 1) and increases the stability of the F91, L128, and F173 regions toward chemical denaturation, Figure 5. The overall structure of Mg^{2+}-CIB1 appears to be very similar to Ca^{2+}-CIB1, especially within the N-lobe, Figure 2. The Mg^{2+}-induced changes in F91W and F173W fluorescence, and the elevated stability of these two regions to chemical denaturation, are clear indications that Mg^{2+}-induced conformational changes in EF-III are communicated to the partner EF-IV domain, as well as EF-II of the N-lobe. However, the exchange behavior for much of the EF-IV domain remains distinct from EF-I−EF-III (Figure 2B), suggesting that the pair of C-lobe EF-hands do not completely behave as a structurally coupled unit. Since the NMR-observable C-lobe residues including those from EF-IV have $\{^1H\}-^{15}N$ NOE values typical for a rigid folded domain (Figure 2D), the W128 and W173 reporter groups are well shielded from the solvent (Figure 4, Table 1) and the α-helical content of Mg^{2+}-CIB1 is nearly identical to that of Ca^{2+}-CIB1 (Supplementary Figure 2 and ref *4*), we suggest that the exchange broadened regions in the C-lobe of Mg^{2+}-CIB1 undergo only small structural fluctuations and are not "unfolded". Accordingly, the chemical denaturation data clearly show that the structure of the F173 region is quite stable in the absence of urea, and even at low [urea], Figure 5F. Like apo-CIB1, the F34 region is the most stable part of the Mg^{2+}-CIB1 protein, and the N → U transition for the F173 region coincides with an N → I transition in the F91 region, Figure 6B. Also like apo-CIB1, all structure (N and I) is lost in Mg^{2+}-CIB1 as the F34 region unfolds near ~5 M urea. However, with Mg^{2+}-CIB1 we were able to identify distinct N → I and I → U transitions in the L128 region, whereas the presence of a transient intermediate conformation in the L128 region of apo-CIB1 could only be implied by the small **m** value in the apo-L128W data (Table 2), but could not be resolved.

Although the structures of Mg^{2+}-CIB1 and Ca^{2+}-CIB1 are quite similar, the higher Ca^{2+} than Mg^{2+} affinity of EF-III and EF-IV results in a Ca^{2+}-loaded structure that is substantially more stable to chemical denaturation than the Mg^{2+}-loaded form, Figure 6C. Ca^{2+} binding to EF-IV also eliminates the conformation exchange in this fourth EF-hand domain (*3*), and the greater stability of the C-lobe is transmitted into an enhanced stability for both EF-II and the more distant EF-I domain in the N-lobe through interlobe interactions, Figure 5. With Ca^{2+}-CIB1, the F34 and L128 regions begin to unfold between ~ 4 and 6 M urea, and this induces an intermediate conformation in the F91 region, Figure 6C. Meanwhile the F173 region remains largely intact presumably due to the Ca^{2+} ion bound strongly to the EF-IV loop just preceding F173. Between ~ 6 and 8 M urea the transient intermediate structure in the F91 region and the native structure of the F173 region completely unfold to yield the fully denatured form of the protein, Figure 6C.

It is clear from the model in Figure 6 that the denaturation of CIB1 does not follow a simple two-state approximation. Rather, the data suggests that the unfolding pathway for CIB1 involves the transient formation of intermediate conformational states, which are likely influenced by the presence of independent folding nuclei with distinct stabilities in different regions of CIB1. In all three forms of CIB1 (apo-, Mg^{2+}-bound, and Ca^{2+}-bound), the N-terminal F34 region in EF-I appears to be one such folding nucleus, having a stability that is distinct from the other EF-hands including the paired EF-II domain. With apo-CIB1 this F34 region is the most stable part of the protein, whereas the metal-free C-lobe is less stable. The Mg^{2+}- or Ca^{2+}-loaded loops of EF-III and EF-IV are also considered to be folding nuclei for Mg^{2+}-

CIB1 and Ca^{2+}-CIB1, respectively, and the binding of these metal ions locks the entire protein, including the intervening EF-II domain, into a more stable structure from the other end. A recent study on a structurally similar 4-EF-hand protein NCS1 has also reported the presence of multiple intermediate conformations along the unfolding pathway, with at least 3 transient intermediates for apo-NCS1 and at least 4 intermediates for Ca^{2+}-NCS1 (*27*). This suggests that related EF-hand proteins also have regions with different stabilities that are influenced by metal coordination at the EF-hand domains. Folding nuclei have been identified in numerous other non-EF-hand proteins as well, and are generally believed to be important for rapid and proper protein folding (*28*, *29*). With CIB1, the presence of a folding nucleus at the N-terminal end might be important to reduce aggregation or early proteolysis of the protein during translation or under conditions of low Mg^{2+} or Ca^{2+} concentrations *in vivo*.

It is also apparent from the present data that the communication between the paired EF-hands in CIB1 is distinct from the ancestral proteins CaM and troponin C (TnC). With CaM and TnC the paired EF-hands in the individual N-lobe (EF-I/EF-II) and C-lobe (EF-III/EF-IV) behave in a largely cooperative manner with respect to metal ion binding, conformational changes, and target protein interactions, while the N- and C-lobes themselves are largely independent and retain similar properties in isolation (*30*−*33*). In contrast, the binding of Mg^{2+} or Ca^{2+} to EF-III or EF-IV of CIB1 is largely independent, interactions between the paired EF-hand domains occur but are less cooperative, and there is substantial communication between the N- and C-lobes of the protein. The interlobe interactions might be necessary for stability and maintaining a native structure in CIB1 including the proper N- and C-lobe orientation, since the binding site for some target proteins, such as the αIIb integrin, spans both lobes of CIB1 (*3*). The noncooperative Mg^{2+}- and Ca^{2+}-binding behavior might also be important for the binding and regulation of some target proteins by CIB1. It has already been shown that CIB1 has more than one distinct binding site for different target proteins (*34*) and that the metal-dependence of various CIB1-target protein interactions can vary, with Ca^{2+}-dependent (*35*), Ca^{2+}-independent (*36*), and Ca^{2+}- or Mg^{2+}-dependent (*8*) interactions being demonstrated. Characterizing the importance of the individual EF-hand domains in these various target protein interactions is an important area to focus future research.

ACKNOWLEDGMENT

The authors wish to thank Drs. Hiroaki Ishida and Deane D. McIntyre for assistance with NMR spectral acquisition and analysis.

SUPPORTING INFORMATION AVAILABLE

One table and three figures as described in the text. This material is available free of charge via the Internet at http://pubs.acs.org.

REFERENCES

1. Yamniuk, A. P., and Vogel, H. J. (2006) Insights into the structure and function of calcium- and integrin-binding proteins, *Calcium Binding Proteins 1*, 150−155.
2. Stabler, S. M., Ostrowski, L. L., Janicki, S. M., and Monteiro, M. J. (1999) A myristoylated calcium-binding protein that preferentially interacts with the Alzheimer's disease presenilin 2 protein, *J. Cell Biol. 145*, 1277−1292.
3. Yamniuk, A. P., Ishida, H., and Vogel, H. J. (2006) The interaction between calcium- and integrin-binding protein 1 and the (alpha)-IIb integrin cytoplasmic domain involves a novel C-terminal displacement mechanism, *J. Biol. Chem. 281*, 26455−26464.
4. Yamniuk, A. P., Nguyen, L. T., Hoang, T. T., and Vogel, H. J. (2004) Metal ion binding properties and conformational states of calcium- and integrin-binding protein, *Biochemistry 43*, 2558−2568.
5. Grabarek, Z. (2006) Structural basis for diversity of the EF-hand calcium-binding proteins, *J. Mol. Biol. 359*, 509−525.
6. Nelson, M. R., and Chazin, W. J. (1998) Structures of EF-hand Ca(2+)-binding proteins: diversity in the organization, packing and response to Ca2+ binding, *Biometals 11*, 297−318.
7. Gentry, H. R., Singer, A. U., Betts, L., Yang, C., Ferrara, J. D., Sondek, J., and Parise, L. V. (2005) Structural and biochemical characterization of CIB1 delineates a new family of EF-hand-containing proteins, *J. Biol. Chem. 280*, 8407−8415.
8. Yamniuk, A. P., and Vogel, H. J. (2005) Calcium- and magnesium-dependent interactions between calcium- and integrin-binding protein and the integrin alphaIIb cytoplasmic domain, *Protein Sci. 14*, 1429−1437.
9. Aitio, H., Laakso, T., Pihlajamaa, T., Torkkeli, M., Kilpelainen, I., Drakenberg, T., Serimaa, R., and Annila, A. (2001) Characterization of apo and partially saturated states of calerythrin, an EF-hand protein from S, erythraea: a molten globule when deprived of Ca(2+), *Protein Sci. 10*, 74−82.
10. Ames, J. B., Dizhoor, A. M., Ikura, M., Palczewski, K., and Stryer, L. (1999) Three-dimensional structure of guanylyl cyclase activating protein-2, a calcium-sensitive modulator of photoreceptor guanylyl cyclases, *J. Biol. Chem. 274*, 19329−19337.
11. Christova, P., Cox, J. A., and Craescu, C. T. (2000) Ion-induced conformational and stability changes in Nereis sarcoplasmic calcium binding protein: evidence that the APO state is a molten globule, *Proteins 40*, 177−184.
12. Gombos, Z., Durussel, I., Ikura, M., Rose, D. R., Cox, J. A., and Chakrabartty, A. (2003) Conformational coupling of Mg2+ and Ca2+ on the three-state folding of calexcitin B, *Biochemistry 42*, 5531−5539.
13. Osawa, M., Dace, A., Tong, K. I., Valiveti, A., Ikura, M., and Ames, J. B. (2005) Mg2+ and Ca2+ differentially regulate DNA binding and dimerization of DREAM, *J. Biol. Chem. 280*, 18008−18014.
14. Wingard, J. N., Chan, J., Bosanac, I., Haeseleer, F., Palczewski, K., Ikura, M., and Ames, J. B. (2005) Structural analysis of Mg2+ and Ca2+ binding to CaBP1, a neuron-specific regulator of calcium channels, *J. Biol. Chem. 280*, 37461−37470.
15. Cox, J. A., Durussel, I., Comte, M., Nef, S., Nef, P., Lenz, S. E., and Gundelfinger, E. D. (1994) Cation binding and conformational changes in VILIP and NCS-1, two neuron-specific calcium-binding proteins, *J. Biol. Chem. 269*, 32807−32813.
16. Gutierrez-Ford, C., Levay, K., Gomes, A. V., Perera, E. M., Som, T., Kim, Y. M., Benovic, J. L., Berkovitz, G. D., and Slepak, V. Z. (2003) Characterization of tescalcin, a novel EF-hand protein with a single Ca2+-binding site: metal-binding properties, localization in tissues and cells, and effect on calcineurin, *Biochemistry 42*, 14553−14565.
17. Peshenko, I. V., and Dizhoor, A. M. (2006) Ca2+ and Mg2+ binding properties of GCAP-1, Evidence that Mg2+-bound form is the physiological activator of photoreceptor guanylyl cyclase, *J. Biol. Chem. 281*, 23830−23841.
18. Zot, H. G., and Potter, J. D. (1982) A structural role for the Ca2+-Mg2+ sites on troponin C in the regulation of muscle contraction, Preparation and properties of troponin C depleted myofibrils, *J. Biol. Chem. 257*, 7678−7683.
19. Masino, L., Martin, S. R., and Bayley, P. M. (2000) Ligand binding and thermodynamic stability of a multidomain protein, calmodulin, *Protein Sci. 9*, 1519−1529.
20. Greene, R. F., and Pace, C. N. (1974) Urea and guanidine hydrochloride denaturation of ribonuclease, lysozyme, alpha-chymotrypsin, and beta-lactoglobulin, *J. Biol. Chem. 249*, 5388−5393.
21. Sobczak, A., Blazejczyk, M., Piszczek, G., Zhao, G., Kuznicki, J., and Wojda, U. (2005) Calcium-binding calmyrin forms stable covalent dimers in vitro, but in vivo is found in monomeric form, *Acta Biochim. Pol. 52*, 469−476.

22. Weljie, A. M., Yamniuk, A. P., Yoshino, H., Izumi, Y., and Vogel, H. J. (2003) Protein conformational changes studied by diffusion NMR spectroscopy: application to helix-loop-helix calcium binding proteins, *Protein Sci. 12*, 228−236.
23. Fraczkiewicz, R., and Braun, W. (1998) Exact and efficient analytical calculation of the accessible surface areas and their gradients for macromolecules, *J. Comput. Chem. 19*, 319−333.
24. Kellis, J. T., Nyberg, K., and Fersht, A. R. (1989) Energetics of complementary side-chain packing in a protein hydrophobic core, *Biochemistry 28*, 4914−4922.
25. Serrano, L., Horovitz, A., Avron, B., Bycroft, M., and Fersht, A. R. (1990) Estimating the contribution of engineered surface electrostatic interactions to protein stability by using double-mutant cycles, *Biochemistry 29*, 9343−9352.
26. Matei, E., Miron, S., Blouquit, Y., Duchambon, P., Durussel, I., Cox, J. A., and Craescu, C. T. (2003) C-terminal half of human centrin 2 behaves like a regulatory EF-hand domain, *Biochemistry 42*, 1439−1450.
27. Muralidhar, D., Jobby, M. K., Krishnan, K., Annapurna, V., Chary, K. V., Jeromin, A., and Sharma, Y. (2005) Equilibrium unfolding of neuronal calcium sensor-1: N-terminal myristoylation influences unfolding and reduces protein stiffening in the presence of calcium, *J. Biol. Chem. 280*, 15569−15578.
28. Fersht, A. R. (1997) Nucleation mechanisms in protein folding, *Curr. Opin. Struct. Biol. 7*, 3−9.
29. Galzitskaya, O. V., Ivankov, D. N., and Finkelstein, A. V. (2001) Folding nuclei in proteins, *FEBS Lett. 489*, 113−118.
30. Drakenberg, T., Forsen, S., Thulin, E., and Vogel, H. J. (1987) The binding of Ca2+, Mg2+ and Cd2+ to tryptic fragments of skeletal muscle troponin C, Cadmium-113 and proton NMR studies, *J. Biol. Chem. 262*, 672−678.
31. Findlay, W. A., Sonnichsen, F. D., and Sykes, B. D. (1994) Solution structure of the TR1C fragment of skeletal muscle troponin-C, *J. Biol. Chem. 269*, 6773−6778.
32. Martin, S. R., and Bayley, P. M. (1986) The effects of Ca2+ and Cd2+ on the secondary and tertiary structure of bovine testis calmodulin, A circular-dichroism study, *Biochem. J 238*, 485−490.
33. Thulin, E., Andersson, A., Drakenberg, T., Forsen, S., and Vogel, H. J. (1984) Metal ion and drug binding to proteolytic fragments of calmodulin: proteolytic, cadmium-113, and proton nuclear magnetic resonance studies, *Biochemistry 23*, 1862−1870.
34. Tsuboi, S., Nonoyama, S., and Ochs, H. D. (2006) Wiskott-Aldrich syndrome protein is involved in alphaIIb beta3-mediated cell adhesion, *EMBO Rep. 7*, 506−511.
35. Leisner, T. M., Liu, M., Jaffer, Z. M., Chernoff, J., and Parise, L. V. (2005) Essential role of CIB1 in regulating PAK1 activation and cell migration, *J. Cell Biol. 170*, 465−476.
36. Blazejczyk, M., Wojda, U., Sobczak, A., Spilker, C., Bernstein, H. G., Gundelfinger, E. D., Kreutz, M. R., and Kuznicki, J. (2006) Ca2+-independent binding and cellular expression profiles question a significant role of calmyrin in transduction of Ca2+-signals to Alzheimer's disease-related presenilin 2 in forebrain, *Biochim. Biophys. Acta 1762*, 66−72.

BI700200Z